ROYAL SOCIETY OF CHEMISTRY

PAPER

Check for updates

Superior electrical conduction of a water repelling 3D interconnected nano-network†

Satyanarayan Dhal,[a] Pritam Das,[a] Manoj K. Rajbhar,[a] Wolfhard Möller,[b] Sriparna Chatterjee, [ID][c] Niranjan Ramgir[d] and Shyamal Chatterjee [ID] *[a]

A three-dimensional (3D) network of interconnected nanowires of functional materials possesses huge potential for device fabrication since it hinders sluggish interfacial charge carrier transport owing to reduced contact resistance. In the present work, the formation of a highly porous 3D interconnected nano-network by Na^+ ion irradiation is demonstrated. The mechanism of solid junction formation at very low energy is established using the results obtained from TRI3DYN computer simulation studies. The formation of a 3D interconnected network resulted in a significant improvement in the electrical conduction as compared to that observed for the pristine nanotube mesh. Further, contact angle measurement shows a transition from "superhydrophilic" nature, as observed for pristine nanotubes, to "superhydrophobic" nature for the 3D nano-network. The superhydrophobicity of the 3D nano-network is expected to find application in miniaturized electronic devices, wherein water condensation and related effects such as short-circuits and erroneous signal output can be significantly minimized.

1. Introduction

In past decades a major focus was on the growth and fabrication of nanostructured functional materials with different morphologies. At present emphasis is being given to using these nanostructured materials to fabricate devices. For such device fabrication, one of the most important aspects would be the joining of individual nanostructures. It is believed that the most flexible way of fabricating a nanoscale junction is a bottom-up approach.[1,2] Many elaborate studies have been performed on the joining of metal[3,4] and carbon based[5,6] nanostructured components. Very recently, our group has shown that ion irradiation can be used effectively for joining ceramic nanowires, producing a 2D interconnected large-scale network.[7–9] An important challenge still remains to realize a stable 3D interconnected network of ceramic nanomaterials. To the best of our knowledge until now there has been no report of the production of a 3D

interconnected nano-network of ceramic nanomaterials by ion irradiation. A handful of papers are available on 3D nanomaterials which have been grown using mainly chemical routes for carbon based[10–13] and a few ceramics based[14,15] nanomaterials. Ion irradiation has been used to fabricate 3D folding sheets[2] and a 3D fin array.[16] The present work on a 3D interconnected nano-network is expected to have versatile applications for miniaturized electronic devices, sensors, filters, catalysts *etc.* The formation of interconnections reduces contact resistance, and as a result an enhancement in charge carrier transport is expected, which in turn will enhance the efficiency of the nanodevices. The large specific surface area or the improved surface area to volume ratio of the 3D network structure may make it useful as a catalyst support.

   In this work, we report the formation of a 3D assembly of hydrogen titanate nanotubes upon ion irradiation. Irradiation of the as-prepared nanotubes with 5 keV Na^+ ions at different ion fluences resulted in the formation of a complex interconnected network, establishing a 3D porous structure. *I–V* measurements revealed that the 3D interconnected nano-network structures exhibit significant enhancement of current conduction as compared to that of the pristine sample. Remarkably, the as-prepared hydrogen titanate nanotubes were superhydrophilic in nature, while the 3D nano-network structure turns out to be superhydrophobic. Our study shows that the fabrication of a 3D interconnected nano-network using ion irradiation is simple, speedy, easily controllable and can be performed at a large scale.

[a] School of Basic Sciences, Indian Institute of Technology Bhubaneswar, Jatni, Khordha, 752050, India. E-mail: shyamal@iitbbs.ac.in
[b] Institute of Ion Beam Physics and Materials Research, Helmholtz-Zentrum Dresden-Rossendorf, 01328 Dresden, Germany
[c] CSIR-Institute of Minerals and Materials Technology, Acharya Vihar, Bhubaneswar, 751013, India
[d] Technical Physics Division, Bhabha Atomic Research Centre, Mumbai, India
† Electronic supplementary information (ESI) available: The videos for time variations of water droplet on the surfaces of pristine hydrogen titanate mesh (V1) and the irradiated 3D network sample (V2) are provided. See DOI: 10.1039/c7tc05374f

This journal is © The Royal Society of Chemistry 2018

J. Mater. Chem. C, 2018, **6**, 1951–1958 | 1951

2. Experimental details

2.1 Synthesis of nanotubes

Hydrogen titanate nanotubes (HTNT) were synthesised hydrothermally. For this synthesis, 99.9% pure TiO_2 (anatase) powder was dissolved in 10 M NaOH solution and stirred continuously for over 3 days. The solution was then put in an autoclave and the growth was carried out at a temperature of 150 °C for about 12 h in a hot-air oven. The product obtained in a powder form was further washed multiple times using dilute hydrochloric acid to remove sodium ions, which produces hydrogen titanate nanotubes (HTNT) as the final product. The HTNT powder was finally washed with deionized water and dried. In order to make the coating, the HTNTs were dispersed in ethanol and ultra-sonicated for 30 min. The ultrasonicated HTNT were drop-casted using a fine-tip pipette on pre-cleaned silicon substrates and dried in air.

2.2 Ion irradiation and characterizations

The irradiation was performed in an ion–solid interaction setup developed in-house at IIT Bhubaneswar.[17] Na+ ions of energy 5 keV were derived from an alkali metal ion source (Kimball Physics Inc.) to irradiate the samples at different ion fluences. The beam was uniform, having a diameter of about 1 cm and a steady beam current of 1 µA. The samples coated on the silicon substrate were mounted on an indigenously developed 5-axis manipulator. The pre- and post-irradiated samples were characterized using a scanning electron microscope (SEM, Zeiss Merlin Compact Gemini) to analyze the surface morphology. A Raman scattering study was performed using a Jobin Yvon T64000 Micro-Raman spectrometer equipped with an inverted microscope. I–V characteristics were studied using a two-probe method. Two tungsten probes were connected to the surface of the sample using silver paste. The current was measured by varying the voltage in the range of ±1 V using a Keithley 6517B electrometer. The wetting properties of pre- and post-irradiated samples were studied by measuring contact angles of sessile drops of Milli-Q water using a contact angle meter (OCA15EC, Dataphysics) at room temperature. The contact angle measurements were done at three different locations on each sample to check the consistency.

3. Simulation details

The computer simulation of ion irradiation effects on 3D HTNT was performed using TRI3DYN, which is based on the Binary Collision Approximation (BCA) and treated using a Monte Carlo concept.[18,19] Unlike the Transport of Ions in Matter (TRIM)[20] program, the current simulation can be performed for a 3D structure with an arbitrary shape, which predicts more accurate post-collision consequences. The target was comprised of volume elements of size 400 (depth) × 600 × 600 nm³ and total of 40 × 60 × 60 voxels with periodic y–z boundaries. A uniform and broad beam of Na+ ions (atomic number 11 and atomic mass 22.98 u) was used as the projectile at an energy of 5 keV and ion fluences of 5×10^{15} and 1×10^{16} ions per cm² respectively.

4. Results and discussions

The as-prepared HTNT show a 3D assembly of loosely bound nanotubes, as observed under a scanning electron microscope (Fig. 1). The size of the 3D clusters is typically in the range between 1 and 10 µm. The transmission electron microscope images of a few nanotubes taken from the 3D cluster reveal that the individual HTNT units are highly crystalline in nature with a typical diameter of 15 ± 5 nm and a length of about 1–2 µm. It is further evident from the figure that the nanotubes are loosely touching each other, possibly due to van der Waals type interactions and, apparently, there is no solid mechanical joining.

The pristine 3D assemblies were irradiated with 5 keV Na+ ions at different ion fluences. At an ion fluence of 1×10^{16} ions per cm² the nanotubes are welded and form large-scale junctions (Fig. 2(a) and (b)) yielding a 3D interconnected network with solid junctions. At a larger ion fluence of 2×10^{16} ions per cm² the junction areas thicken, as shown in Fig. 2(c) and (d). The 3D network structure is
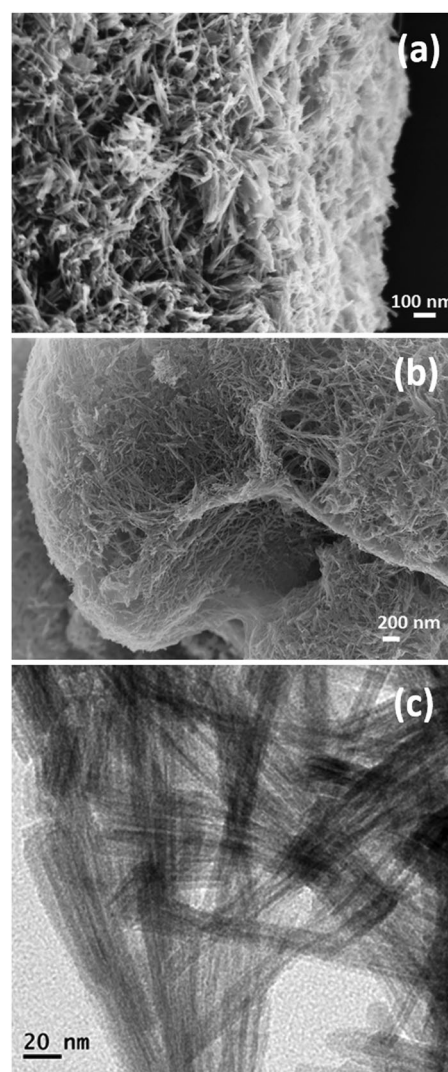

Fig. 1 (a and b) Scanning electron micrographs and (c) high resolution TEM image of the 3D pristine hydrogen titanate nanotube assembly.
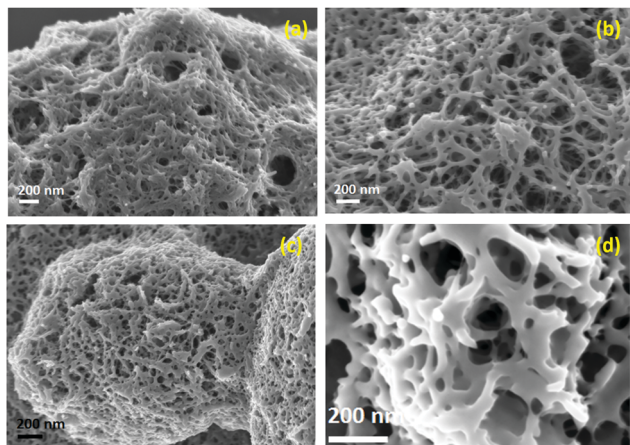
Fig. 2 SEM micrographs of 3D HTNT samples irradiated with 5 keV Na^+ ions at fluences of 1×10^{16} ions per cm^2 (a), (b) and 2×10^{16} ions per cm^2 (c), (d).

comprised of pores of sizes in the range of 20–200 nm. This observation clearly implies that using low-energy ions a 3D welded nano-network with a porous structure can be achieved easily. The joining of the 3D network at a fluence of 2×10^{16} ions per cm^2 is further investigated using TEM. This apparently shows two effects: namely, nanotubes have been converted into solid nanowires and a clear physical join persists between them (Fig. 3).

The joining mechanism at this low energy, where thermal spike related effects are less likely, is investigated by employing TRI3DYN simulations. The collisional effects can be realized through this simulation while looking into the evolutions of atomic fractions of the nanotubes before and after irradiation. For instance, in Fig. 4(a) and (b), the titanium atomic fraction is shown on two HTNT oriented perpendicular to each other in a 3D geometry. With an increase in ion fluence from 5×10^{15} up to 1×10^{16} ions per cm^2 (Fig. 4(c) and (d)) a consistent downward flow (along the direction of ions) of titanium atoms occurs due to recoils and sputtering. The ion irradiation further
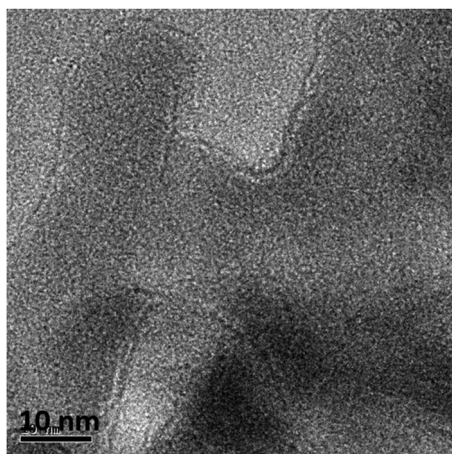

Fig. 3 High resolution TEM image of 3D HTNT irradiated with 2×10^{16} ions per cm^2 showing welded junctions.

creates dangling bonds due to collision-induced defects on the surface of the nanotubes. Thus, the amassed atoms in between two nanotubes bridge the gap by saturating the dangling bonds and establish a solid join.[9] The simulation further shows that the hollow part of the nanotubes is gradually filled with atoms, producing a solid wire-like structure, as is also evident in the TEM image (Fig. 3). The simulation predicts a change in the Ti/O ratio with increasing ion fluence (Fig. 5(a) and (b)). It is apparent that the Ti/O ratio increases mostly in the lower nanotubes of the given geometry from an initial 0.42 to about 0.8, which indicates the role of preferential sputtering and surface diffusion.[8,9] Such altered abundances of Ti and O may trigger the formation of a new phase of titanium oxide. The simulation also predicts that some negligible amount of silicon gets deposited only at the bottom of the nanotubes (Fig. 5(c) and (d)). Silicon atoms from the substrate are ejected due to sputtering, which is caused by primary ions as well as by recoiled atoms. The sputtered-out silicon atoms are slow enough and, therefore, they settle at the bottom part of the nanotubes. TRI3DYN simulation shows that the atomic fraction of silicon at the bottom of the nanotubes is nearly 0.2. The primary Na^+ ions travel across the nanotube walls and suffer successive collisions with the lattice atoms and lose energy mostly through nuclear stopping (i.e. elastic collision). We have performed a calculation using the TRIM[20] program to simulate the collision details, which shows that the Na^+ ions have range of about 8 nm. Since the average wall thickness of a nanotube is 5 nm, the ions are mostly stopped on the opposite side of the wall of entry as well as just outside the nanotube: i.e. in the junction areas. The TRI3DYN simulation confirms the presence of most of the sodium atoms at the sidewall and junction areas, as seen in Fig. 5(e) and (f). The simulation results in Fig. 4 and 5 further show that the bottoms of the nanotubes are physically welded to the substrate, which offers the possibility that the irradiated titanate surface can be used as a coating material.

The irradiation-induced formation of a new phase is also apparent in the Raman scattering study. As shown in Fig. 6, the pristine sample shows characteristic peaks at around 198, 272. 458 and 678 cm^{-1} that correspond to the hydrogen titanate nanotubes. At the largest ion fluence used in this study several strong peaks appear. Apart from the peak at 272 cm^{-1} for hydrogen titanate, peaks around 440 and 612 cm^{-1} correspond to the rutile phase and the peak around 150 cm^{-1} corresponds to the anatase phase of titanium dioxide.[21]

4.1 Electrical property

I–V measurements for pristine and irradiated 3D samples show interesting aspects (Fig. 7). For pristine HTNT the current has been measured in the voltage range of −1 to +1 V, which yields a nonlinear curve with current in the range of 3–5 µA (Fig. 7(a)). The current increases drastically at an ion fluence where large-scale welding is formed and it reaches about 10 mA at a fluence of 2×10^{16} ions per cm^2 (Fig. 7(b)). The distance between the two tungsten probes was fixed at 4 mm for both pristine and irradiated samples. Each probe has a width about 2 mm. While the conductivity of the pristine sample is estimated to
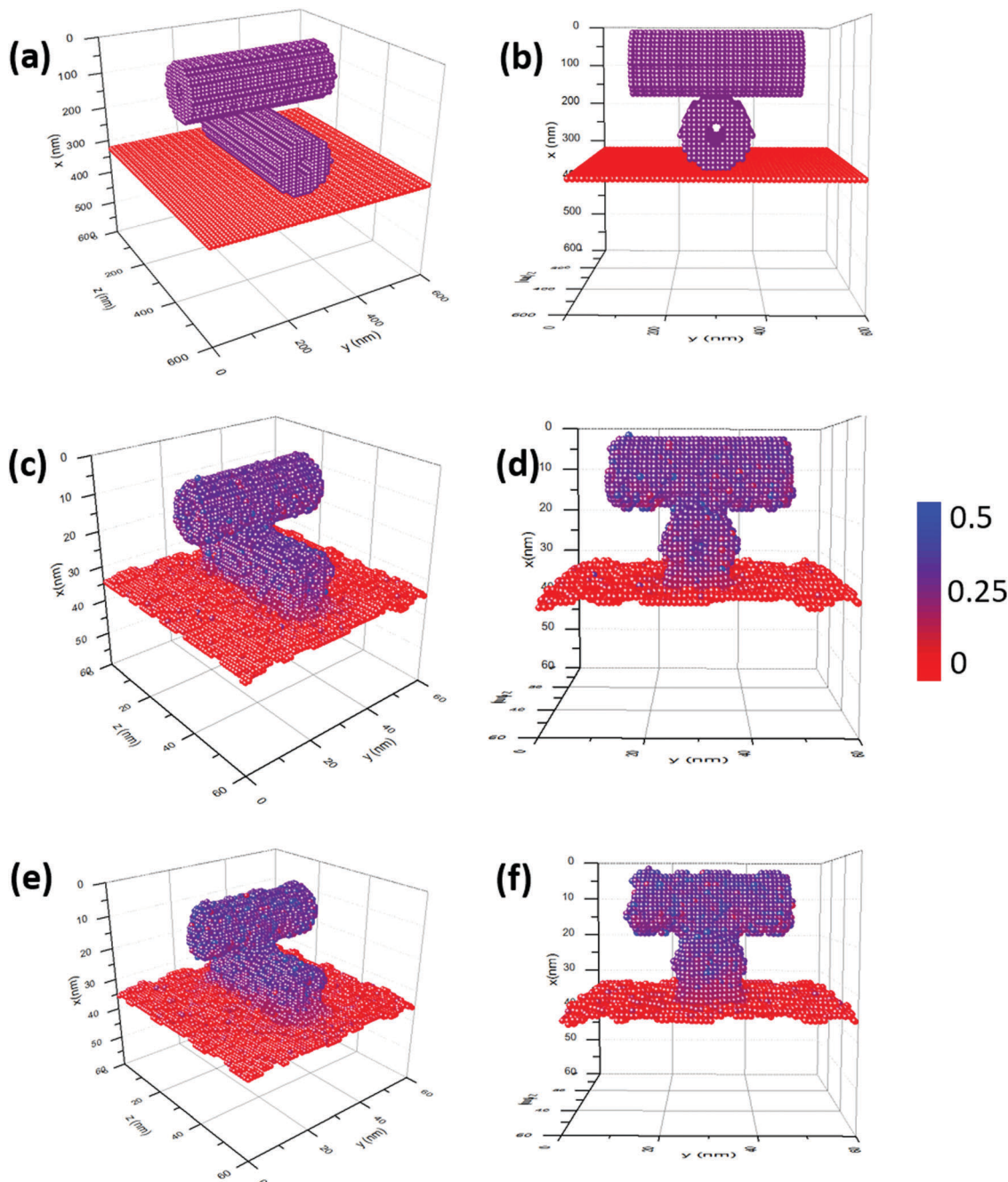
This journal is © The Royal Society of Chemistry 2018

J. Mater. Chem. C, 2018, **6**, 1951–1958 | **1953**

Fig. 4 The surface contours as obtained from the TRI3DYN computer simulation show Ti atomic fractions: (a, b) for pristine sample, (c, d) and (e, f) after 5 keV Na$^+$ irradiation at ion fluences of 5×10^{15} ions per cm^2 and 1×10^{16} ions per cm^2, respectively. The outer diameter of the nanotubes is 15 nm with a wall thickness of 5 nm. The Ti atomic fraction is shown in the range from 0 to 0.5.

be 7.86 S m^{-1} at 0.5 V, the value for the irradiated sample is 2.19 × 10^4 S m^{-1}, which is about four orders of magnitude larger than that of the pristine sample. For pristine 3D mesh the nanotubes are loosely connected to each other, which leads to the high contact resistance. In contrast, for the irradiated 3D sample, the nanotubes are physically welded, providing good contacts with a large area, as shown schematically in Fig. 8. Furthermore, the nanotubes are converted into solid nanowires providing high cross section areas for the conduction of charge carriers. Thus the combined effect of welding and conversion into solid nanowires enhances the electrical conductivity and reduces the overall resistance.[6] At high ion fluence (2 × 10^{16} ions per cm^2) the I–V curve tends to become more linear with no barrier potential. Since the work function of silver (4.3 eV[22,23]) is comparable with the electron affinity of titanium oxide, which is in the range of 3.9–4.8 eV,[24–26] this leads to a zero barrier height with almost no rectifying action in this case.
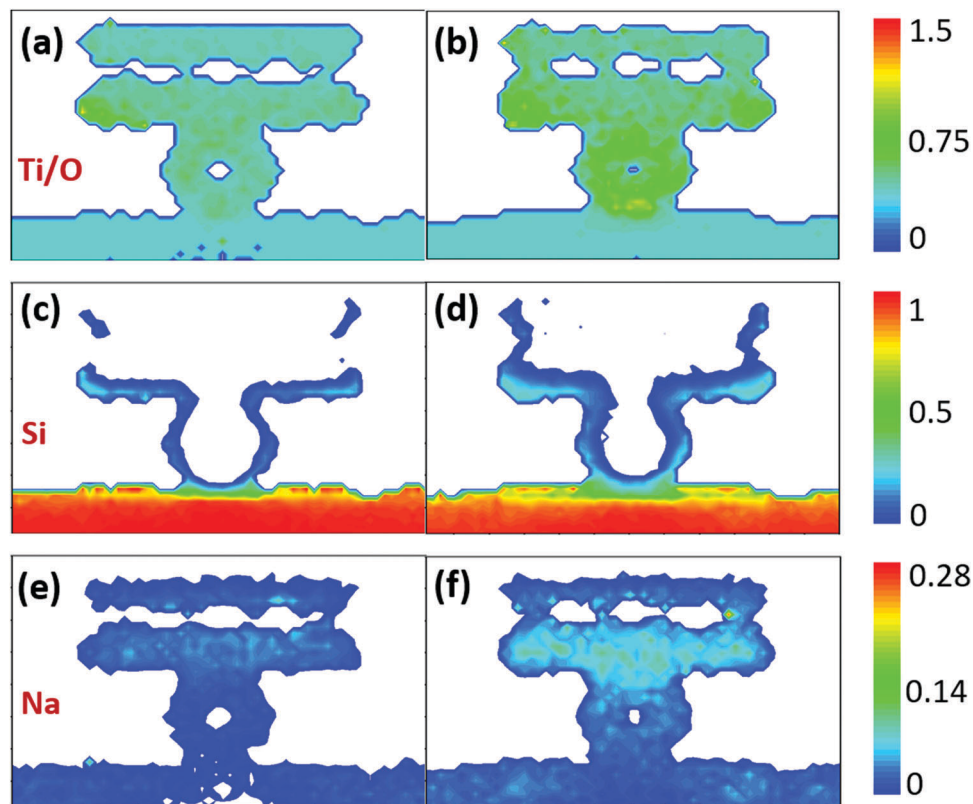
Fig. 5 X–Y cut-through the axis of the upper tube. The Ti/O atomic ratio (a, b); the silicon atomic fraction (c, d) and sodium atomic fractions (e, f) are shown for two different ion fluences of 5×10^{15} ions per cm^2 (left-hand figures) and 1×10^{16} ions per cm^2 (right-hand figures).
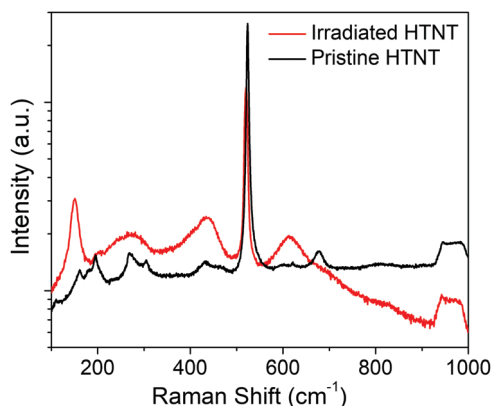

Fig. 6 Raman scattering spectra of pristine and irradiated (2×10^{16} ions per cm^2) samples.

4.2 Wetting property

The interaction of water droplets with both pristine and irradiated 3D samples has been studied using contact angle measurements. The water droplet on the pristine sample disappears extremely fast, as shown in Fig. 9. The time evolution of the droplet has been captured from the initial stage, i.e. before touching the surface. Within 0.15 s the water droplet flattens on the surface with a contact angle close to 0° and it vanishes completely before 5 s. Thus the pristine sample turns out to be superhydrophilic in nature. This, however, changes drastically

upon ion irradiation. As shown in Fig. 10, the contact angle of water increases with increasing ion fluence. At an ion fluence of 8×10^{15} ions per cm^2 the sample surface becomes hydrophilic with a contact angle of $53° \pm 2°$ (Fig. 10(a)) from an initial superhydrophilic surface. At an increased ion fluence of 1×10^{16} ions per cm^2 the sample surface becomes hydrophobic with a contact angle of $105° \pm 2°$ (Fig. 10(b)). At the highest ion fluence of 2×10^{16} ions per cm^2 used in this work, the surface turns superhydrophobic with a contact angle of $150° \pm 2.5°$ (Fig. 10(c)). There was almost no change in the contact angle of the irradiated sample (i.e. superhydrophobic nature) measured two months after the irradiation (Fig. 10(d)). We have delved into possible reasons for such drastic changes.

Usually the wetting property depends on the chemical property of the surface as well as on the microstructures present on the surface. It is known that a monoclinic hydrogen titanate structure contains lot of –OH groups on the surface.[27,28] Thus the presence of OH groups in a pristine sample attracts water molecules, leading to the superhydrophilic nature of the surface. On the other hand, irradiated samples contain rutile and anatase phases, as evident from Raman spectroscopy, which usually yields a hydrophobic surface.[29,30] However, a significant contribution towards a strong water repelling nature comes from the 3D porous network. Usually the roughness of a nanostructured surface leads to a hydrophobic nature, termed a Wenzel surface.[31,32] The other type is a Cassie–Baxter type surface, where trapped air in the nanostructure pushes back
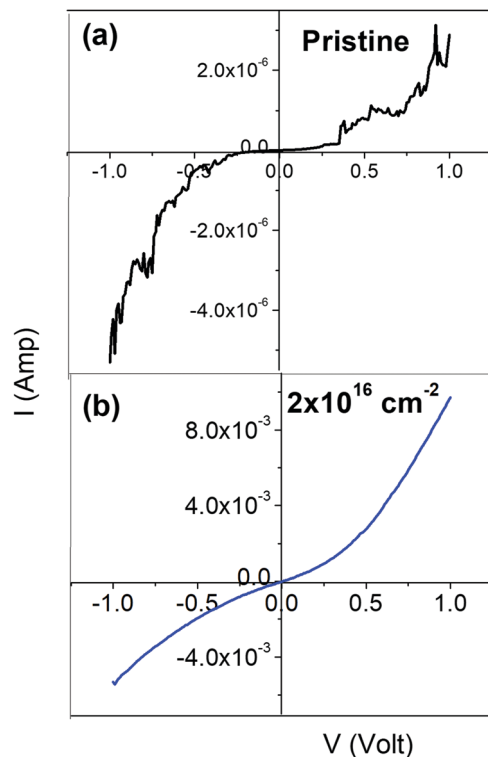
This journal is © The Royal Society of Chemistry 2018

J. Mater. Chem. C, 2018, 6, 1951–1958 | 1955

Fig. 7 $I-V$ curves for pristine (a) and irradiated 3D hydrogen titanate at an ion fluence of 2×10^{16} ions per cm^2 (b).
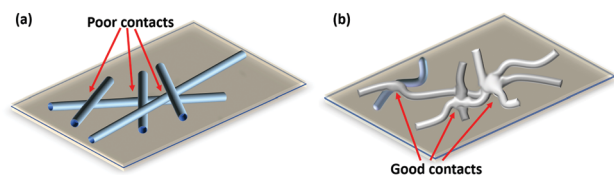

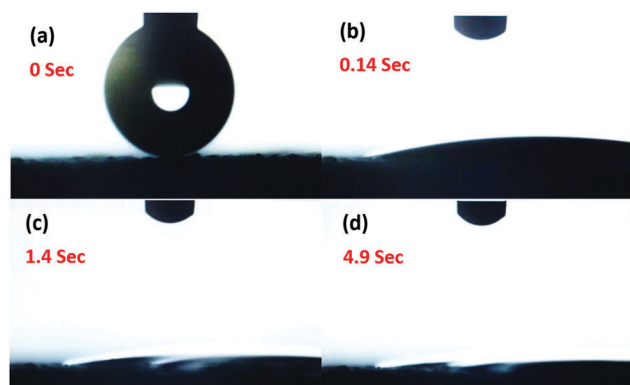Fig. 8 Schematic showing reduced contact resistance and increase in conduction area after the ion irradiation.

Fig. 9 Optical image of water droplet on pristine 3D hydrogen titanate assembly at 0 (a), 0.14 (b), 1.4 (c) and 4.9 s (d).

Fig. 10 Optical image of water droplet on irradiated 3D hydrogen titanate network for ion fluences 8×10^{15} ions per cm^2 (a), 1×10^{16} ions per cm^2 (b), immediately (c) and two months (d) after the ion irradiation at a fluence of 2×10^{16} ions per cm^2.

the water, leading to the superhydrophobic nature of the surface.[32,33] The welded network traps air, which forms a Cassie state,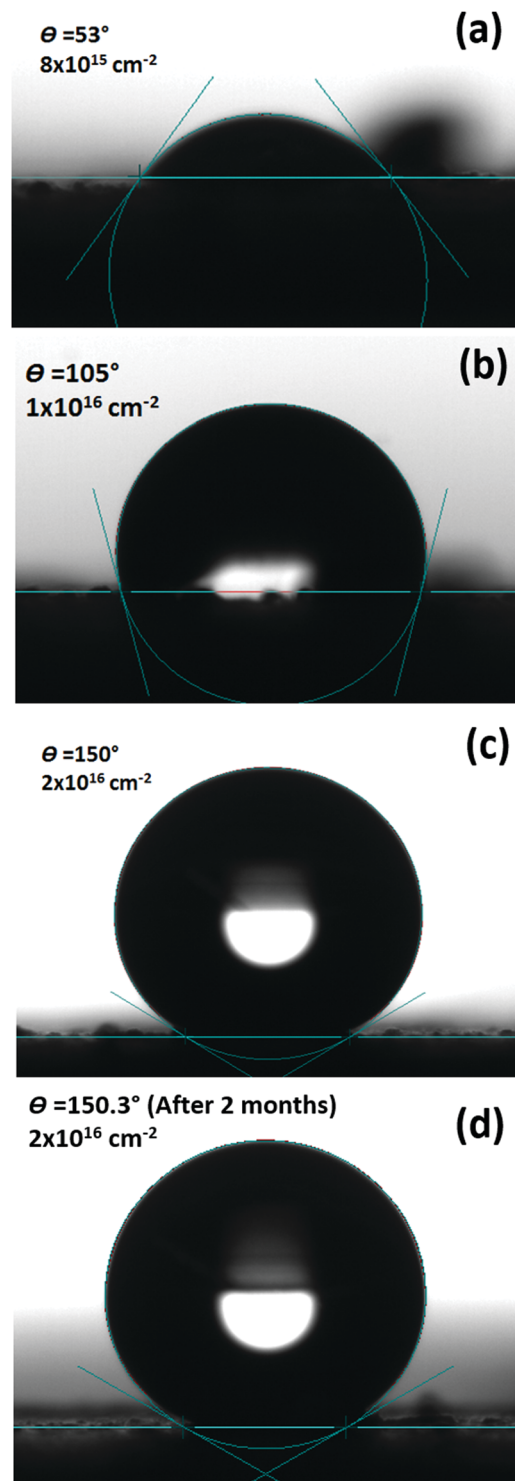 resulting in a hydrophobic nature. With increasing ion fluence, the welding occurs over a large scale and more trapped air pockets are produced, which leads to the super-hydrophobic nature of the surface. We have studied the time evolution of water droplets on the irradiated surfaces for
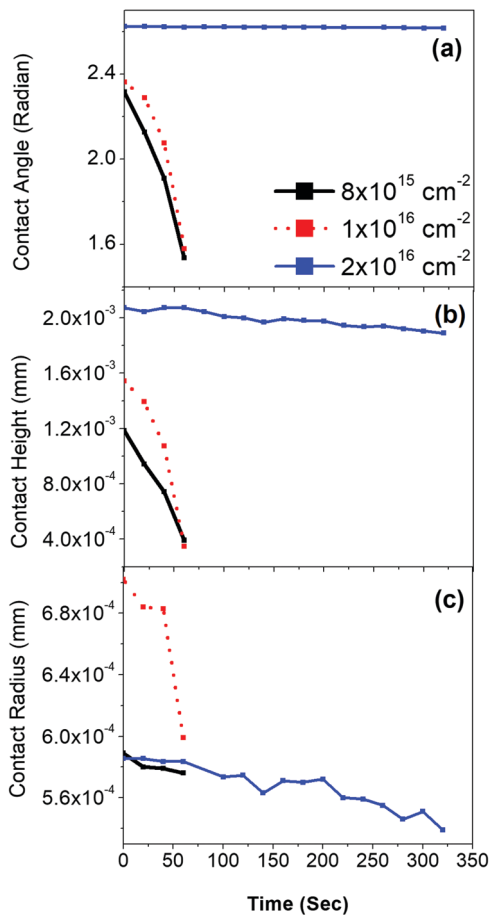
1956 | J. Mater. Chem. C, 2018, 6, 1951–1958

This journal is © The Royal Society of Chemistry 2018

Fig. 11 Time dynamics of contact angle (a), contact height (b) and contact radius (c) of 3D hydrogen titanate samples irradiated at different ion fluences.

different ion fluences, as shown in Fig. 11. It is evident that for lower ion fluences (8×10^{15} and 1×10^{16} ions per cm^2) the contact parameters, such as contact angle (θ), contact height (h) and contact radius (r_b), drop drastically to about 50–70% within 2 min. Whereas, at the highest fluence of 2×10^{16} ions per cm^2, θ, h and r_b remain almost constant for a long time.

The diffusion coefficient (D) was calculated using Fick's law of diffusion for a sessile water droplet.[33,34] For the highest fluence used, this yields a value of $(3.13 \pm 0.52) \times 10^{-5}$ m^2 S^{-1}, which is comparable with the normal evaporation of water droplets into the environment at room temperature.[35] This implies that the irradiated 3D surface acts as a good water repellent. We have further tested the wetting behaviour of the nanowelded surface with saline water (concentration 1%), which showed a superhydrophobic character with a contact angle of about 151° (figure not shown). Thus the water repelling property of the irradiated surface is retained for both normal water and salted water. It may be interesting to note that usually the sodium based compounds are hygroscopic in nature. The network structure supersedes the water-attraction nature of sodium and makes the sample superhydrophobic. In principle, the amount of sodium implanted is tiny and it is mostly inside the surface with an approximate range of 8 nm (as obtained from TRIM simulation). Therefore, sodium plays almost no role in the wetting behaviour of the sample. The dynamics of interaction of the water droplets with the present superhydrophilic and superhydrophobic surfaces are provided in the form of videos in the ESI† as V1 and V2, respectively.

5. Conclusions

In conclusion, low-energy ion irradiation is used as a tool to fabricate a well-interconnected 3D nano-network of titanium oxide based nanowires. The Na$^+$ ion irradiation leads to the formation of nanowires from hollow nanotubes and triggers solid mechanical joining between them. The 3D network structure offers a highly porous structure and is expected to have a large surface area as well as volume. The interconnected network shows about four orders of magnitude enhancement in electrical conductivity compared to that of the pristine sample, which is attributed to the physical joining and the conversion into solid nanowires. Taking into consideration the high surface area and volume with better conduction of charge carriers, this 3D interconnected nano-network could be a potential candidate for sensors or filtering applications. The water contact angle measurements show that the pristine hydrogen titanate nanotubes are superhydrophilic in nature. A drastic transition takes place upon irradiation with Na$^+$ ions. The surface gradually becomes hydrophobic and finally turns superhydrophobic at larger ion fluences. This wetting property provides an advantage for this structure for use as a water-borne corrosion resistive coating.

Conflicts of interest

There are no conflicts to declare.

Acknowledgements

References

1 H. Yan, *et al.*, *Nature*, 2011, **470**(7333), 240–244.
2 W.-H. Kim, *et al.*, *ACS Nano*, 2016, **10**(4), 4451–4458.
3 Z. Gu, *et al.*, *Langmuir*, 2007, **23**(3), 979–982.
4 E. C. Garnett, *et al.*, *Nat. Mater.*, 2012, **11**(3), 241–249.
5 G. Seth Roberts and P. Singjai, *Nanoscale*, 2011, **3**(11), 4503.
6 J. S. Woo, *et al.*, *Sci. Rep.*, 2014, **4**, 4808.
7 S. Dhal, *et al.*, *Nanotechnology*, 2015, **26**(23), 235601.
8 S. Dhal, *et al.*, *AIP Conference Proceedings*, AIP Publishing, 2017, vol. 1832, p. 80091.
9 S. Dhal, *et al.*, *Cryst. Growth Des.*, 2017, **17**(5), 2660–2666.

This journal is © The Royal Society of Chemistry 2018

J. Mater. Chem. C, 2018, **6**, 1951–1958 | **1957**

10 D. P. Hashim, *et al.*, *Sci. Rep.*, 2012, **2**, 363.

11 P. M. Sudeep, *et al.*, *ACS Nano*, 2013, **7**(8), 7034–7040.

12 S. Ozden, *et al.*, *Carbon*, 2017, **119**, 142–149.

13 J. Yan, *et al.*, *Adv. Funct. Mater.*, 2017, **27**, 22.

14 Bin Liu and Hua Chun Zeng, *J. Am. Chem. Soc.*, 2004, **126**(51), 16744–16746.

15 Y. Xia, *et al.*, *J. Alloys Compd.*, 2017, **705**, 58–63.

16 C.-L. Wu, *et al.*, *Nano Lett.*, 2016, **17**(1), 249–254.

17 P. Das, *et al.*, *Nucl. Instrum. Methods Phys. Res., Sect. B*, 2017, **413**, 31–36.

18 W. Möller, *et al.*, *Nucl. Instrum. Methods Phys. Res., Sect. B*, 2014, **322**, 23–33.

19 W. Eckstein, Springer Series in Materials Science, *Computer Simulation of Ion-Solid Interactions*, Springer-Verlag, Berlin, Heidelberg, 1991.

20 J. F. Ziegler and J. P. Biersack, The Stopping and Range of Ions in Matter, *Treatise on Heavy-Ion Science*, Springer US, Boston, MA, 1985, pp. 93–129.

21 Y. Swamy, *et al.*, *Appl. Phys. Lett.*, 2006, **89**(16), 1–4.

22 A. W. Dweydari, *et al.*, *Phys. Status Solidi*, 1975, **27**(1), 223–230.

23 H. B. Michaelson, *J. Appl. Phys.*, 1977, **48**(11), 4729–4733.

24 D. O. Scanlon, *et al.*, *Nat. Mater.*, 2013, **12**(9), 798–801.

25 K. D. Schierbaum, *et al.*, *Sens. Actuators, B*, 1991, **4**(1–2), 87–94.

26 R. Könenkamp, *et al.*, *Mater. Sci. Eng., B*, 2000, **69**, 519–521.

27 S. Chatterjee, *et al.*, *J. Nanomater.*, 2014, **2014**, 328618.

28 A. Liu, *et al.*, *Anal. Chem.*, 2005, **77**(24), 8068–8074.

29 R. Wang, *et al.*, *J. Phys. Chem. B*, 1999, **103**(12), 2188–2194.

30 X. Peng, *et al.*, *Appl. Phys. A: Mater. Sci. Process.*, 2005, **80**(3), 473–476.

31 R. N. Wenzel, *Ind. Eng. Chem.*, 1936, **28**(8), 988–994.

32 S. Dhal, *et al.*, *Soft Matter*, 2015, **11**(47), 9211–9217.

33 A. B. D. Cassie and S. Baxter, *Trans. Faraday Soc.*, 1944, **40**, 546–551.

34 Y.-S. Yu, *et al.*, *J. Colloid Interface Sci.*, 2012, **365**(1), 254–259.

35 R. C. Weast, *et al.*, *CRC Handbook of Chemistry and Physics*, CRC Press, Boca raton FL, 1989, vol. 1990.